Energy Conversion and Management 288 (2023) 117137

Contents lists available at ScienceDirect

Energy Conversion and Management

journal homepage: www.elsevier.com/locate/enconman

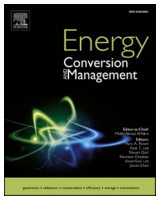

Different strategies in an integrated thermal management system of a fuel cell electric bus under real driving cycles in winter

Alberto Broatch, Pablo Olmeda *, Xandra Margot, Sebastián Aceros

CMT – Motores Térmicos, Universitat Politècnica de València, Camino de Vera s/n 46022, Valencia, Spain

ARTICLE INFO

Keywords:
Electric vehicles
Proton exchange membrane fuel cell
Integrated thermal management systems
Fuel cell electric bus

ABSTRACT

Due to the climate crisis and the restriction measures taken in the last decade, electric buses are gaining popularity in the transport sector. However, one of the most significant disadvantages of this type of vehicle is its low autonomy. Many electric buses with proton-exchange membrane fuel cells (PEMFC) systems have been developed to solve this problem in recent years. These have an advantage over battery-electric buses because the autonomy depends on the capacity of the hydrogen tanks. As with batteries, thermal management is crucial for fuel cells to achieve good performance and prolong service life. For this reason, it is necessary to investigate different strategies or configurations of a fuel cell electric bus's integral thermal management system (ITMS). In the present work, a novel global model of a fuel cell electric bus (FCEB) has been developed, which includes the thermal models of the essential components. This model was used to evaluate different strategies in the FCEB integrated thermal management system, simulating driving cycles of the public transport system of Valencia, Spain, under winter weather conditions. The first strategy was to use the heat generated by the fuel cell to heat the vehicle's cabin, achieving savings of up to 7%. The second strategy was to use the waste heat from the fuel cells to preheat the batteries. It was found that under conditions where a high-power demand is placed on the fuel cell, it is advisable to use the residual heat to preheat the battery, resulting in an energy saving of 4%. Finally, a hybrid solution was proposed in which the residual heat from fuel cells is used to heat both the cabin and the battery, resulting in an energy saving of 10%.

1. Introduction

The transport sector is responsible for about a quarter of the greenhouse gases emitted worldwide, with land transport sub-sector being by far the largest emitter [1]. For this reason, the use of zero-emission land transport vehicles such as electric vehicles have been promoted in recent years [2–4]. However, there are currently many disadvantages in terms of range and charging time with pure battery electric vehicles [5]. Researchers and vehicle manufacturers have been working on alternatives in recent years, such as the fuel cell electric vehicles (FCEV).

FCEVs enjoy great popularity because they are emission-free, have a high energy density and do not have problems with recharging time and autonomy, as is the case with pure battery electric vehicles. On the other hand, this technology has other disadvantages. A suitable infrastructure for hydrogen refueling stations still needs to be created that can supply these vehicles with fuel on a large scale [6]. In addition, the prices for this technology need to be lowered in order to be competitive in the current market [7]. Despite these problems, there is a lot of interest in the use of fuel cells in heavy-duty vehicles, such as city buses. In recent years, fuel cell electric buses (FCEB) have penetrated the electric bus market significantly. With each passing year, their share has increased, making the percentage of FCEBs in electric bus fleets more and more important and narrowing the gap with more established technologies such as hybrid electric buses or battery electric buses [8]. This preference for fuel cells is mainly due to two reasons. First, fuel cells have great potential for applications that require long ranges and high load capacity [9]. The second reason is that the bus fleet is charged at a single location, so only a single charging station is required [10]. Despite these advantages, these vehicles also present complexities, such as their thermal management system, which plays a crucial role.

Almost half of the energy produced by the electrochemical reaction in the fuel cell is not electrical energy but generated heat [11]. The proton-exchange membrane fuel cells (PEMFC) must be kept within the operating temperature range of 60–80 °C. The higher the temperature in that range, the better the performance of the PEMFC system [12]. However, if the operating temperature is very high, the membrane will

* Corresponding author.
E-mail address: pabolgon@mot.upv.es (P. Olmeda).

https://doi.org/10.1016/j.enconman.2023.117137
Received 17 March 2023; Received in revised form 20 April 2023; Accepted 2 May 2023
Available online 9 May 2023

dehydrate, which can lead to the reduction in the proton conductivity of the membrane [13]. For these reasons, the fuel cell thermal management system (FCTMS) deserves special attention. In addition, the vehicle thermal management system (VTMS) has other subsystems, such as the battery thermal management system (BTMS), the motor thermal management system (MTMS) and the heating, ventilation, and air conditioning (HVAC) system. The BTMS is responsible for ensuring that the battery does not reach very high temperatures to avoid the risk of thermal runaway [14]. On the other hand, the BTMS must also ensure that the battery is heated when cold to avoid phenomena such as lithium plating that damage the battery [15]. With MTMS, the only thing to watch out for is that the motor does not reach very high temperatures so that it is not damaged [16]. However, the motor can be operated in a wide range of temperatures, so it is a simple system. In addition, the HVAC system is responsible for thermal comfort inside the vehicle. All these subsystems have their own loops, but so many separate loops can lead to space and weight issues [17]. In addition, many of these subsystems can be integrated among them, especially if the residual heat from one of the subsystems can heat another that needs it, resulting in energy savings [18,19]. Therefore, thermal management systems are crucial in maintaining optimal performance conditions and ensuring the safety of subsystems in FCEVs. They also prevent component degradation, which could drastically reduce the lifespan of the vehicle. For these reasons, studying integrated thermal management systems (ITMS) in FCEVs is of paramount importance.

Several researchers have made significant contributions to ITMS in FCEV in recent years. In a study by Farsi et al. an ITMS was proposed for an FCEV that preheats the PEMFC inlet air by cooling the battery and then directs it to the cathode side of the PEMFC [20]. It was found that the PEMFC using the preheated air can produce 450 W/m^2 higher electrical power density than the baseline configuration without preheating in cold weather conditions. A VTMS with a heat pump system for an FCEV was proposed by Zhao et al [17]. In this study, an analysis of the performance of the thermal management of the cabin was conducted, which concluded that it is beneficial in terms of hydrogen consumption to use the residual heat from the PEMFC as a heat source for the heat pump system. In the work of Yang et al. an ITMS of an FCEV was created with different control strategies and integrated energy management [21]. The simulations were carried out under high temperature driving cycles. The results of this study showed the rationality of the system model and control strategies, which can be helpful in the design and development of this type of vehicle. In a study by Xu et al. an ITMS for a PEMFC vehicle was developed, focusing on the analysis of heat transfer and generation of the motor, PEMFC and charge air [22]. With this proposal, it was possible to keep the temperature of the different components of the vehicle within an optimal range. In the work of Xing et al. a comprehensive model of an ITMS for an FC/battery vehicle was developed [23]. With this model, parametric studies were performed by varying the inlet temperature of the PEMFC coolant and the mass flow rate to analyze the thermal behavior of the PEMFC. A heat pump assisted VTMS was proposed by Kim et al. to improve the cold start performance of FCEVs [24]. For this purpose, models for the PEMFC and the thermal management system were used, which were validated with experimental data. The simulations were performed under different operating conditions to analyze the effects of the critical operating conditions. Longfei et al. propose an ITMS model for an FCEB [25]. Simulations of a modified new European driving cycle were performed with this model, and the performance of the ITMS during cooling and heating was analyzed. The results showed that the ITMS has excellent cooling performance at high temperatures. By utilizing the residual heat at low temperatures, significant savings in hydrogen consumption were also achieved. After reviewing the bibliography, it can be concluded that thermal management in FCEVs is crucial and that more relevant studies need to be conducted in the case of FCEBs. As a result of the current lack of comprehensive and detailed understanding of how different subsystems interact with each other in terms of thermal management, there is a pressing need to develop a global vehicle model that considers the various powertrain submodels for an adequate evaluation. This approach would allow for a better understanding of the interdependence of each subsystem's thermal behavior and enable the design of an integrated thermal management system that considers the entire powertrain. By doing so, it is possible to achieve a more efficient and effective thermal control system, which can lead to significant improvements in the vehicle's overall performance, energy efficiency, and sustainability. Therefore, it is crucial to conduct further research on integrated thermal management systems and develop a comprehensive global vehicle model to fully unlock their potential and improve the performance of fuel cell electric vehicles.

In this study, a novel global model of a PEM fuel cell electric bus was developed. This model considers the main subsystems of the FCEB powertrain, such as the PEMFC, the battery, electric motor, and HVAC system. It also possesses an energy management system to define the operating conditions of the powertrain based on the requirements of the vehicle and various operating variables. A basic configuration was proposed for the VTMS, where the thermal management subsystems are independent of each other, and which was used as a reference. Three other ITMS were proposed that use the residual heat from the PEMFC to heat different vehicle components, such as the battery and the cabin. To evaluate the different ITMS and their potential benefits, simulations were performed for a real driving cycle used by the bus fleet of the public transport system of Valencia, Spain, in winter weather conditions.

2. Methodology

2.1. Considered city bus

The commercial software GT -Suite (v2020, Gama Technology) was used to develop the global FCEB model. This software allows the integration of the individual sub-models of the vehicle and performs transitory simulations of the entire vehicle. Fig. 1 illustrates the FCEB model, which consists of different submodels: PEMFC, battery, and electric machine. Each of these submodels have their own thermal management system. There are also cabin and HVAC submodels, and an energy management system that controls the energy demand of the PEMFC. Inputs required to run the whole model include the driving cycle, ambient temperature, and initialization temperature, while model outputs include energy and hydrogen consumption, and thermal behavior. The global model is constructed to evaluate the benefits of different thermal management strategies and assist in the pre-design of the system. Therefore, global model validation is not performed. However, the models of the most crucial components in the system are validated separately.

Fuel cell vehicles have different powertrain configurations to improve their efficiency and performance. The hybrid dominant battery setup combines the fuel cell system with a battery pack, which supplies power during acceleration and uphill driving, while the fuel cell system provides power during steady-state driving. The series configuration directly connects the fuel cell system to the electric motor for smooth and efficient operation, but it may struggle to keep up with high power demands. The range extender configuration uses a small fuel cell system to provide additional power to the battery pack when it is running low, extending the vehicle's range. Some powertrain structures use supercapacitors to store excess energy from the fuel cell system during low demand periods and use it later when power demands are high.

In this study, a hybrid-dominant battery configuration was selected as it improves the efficiency of the fuel cell system by reducing the load placed on it, resulting in longer operating ranges and better performance. For this work, a 12-meter-long city bus with a capacity of up to 88 passengers was modeled. The bus powertrain consists of a PEM fuel cell stack, a lithium-ion battery pack, and two permanent magnet synchronous motors (PMSMs). Table 1 shows further details of the modeled vehicle.

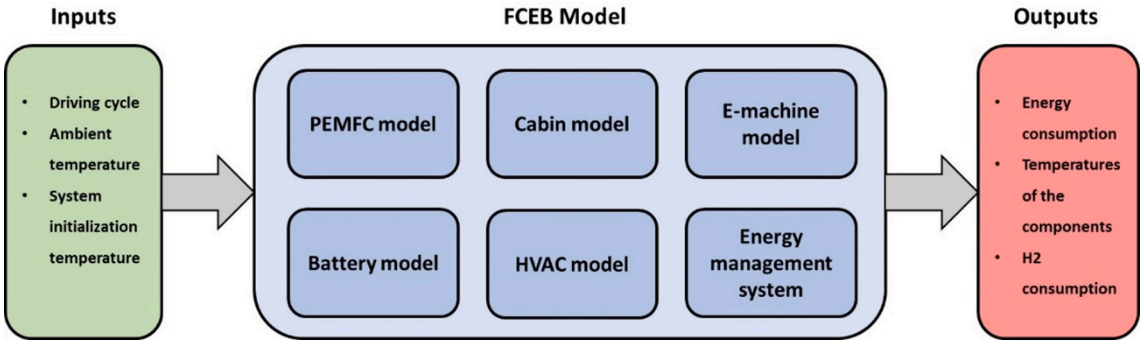

Fig. 1. Diagram of the global model of the FCEB.

Table 1
Vehicle main specifications.

Parameter	Value
Curb Weight (kg)	13,200
Frontal Area (m^2)	7.24
Nominal Tire Width (mm)	275
Diameter of Wheel (in)	22.5
Gear Ratio (-)	21.779
Operating Voltage (V)	512
Battery Capacity (Ah)	200
Max. PMSM Power (kW)	150
Max. PMSM Torque (Nm)	550
Fuel Cell Rated Power (kW)	150

2.2. Battery model

A detailed model of the lithium-ion battery pack is essential for this bus, whose powertrain is dominated by the battery. For the electrical modeling, a first-order equivalent circuit model from the GT -Suite library was used. This model was chosen because it is simple, fast, and easy to integrate, also it is ideal for drive cycle simulations and provides reliable results if its characterization parameters are correctly estimated [26].

The battery cell used in this model was a prismatic aluminum-shell lithium-ion battery with a nominal capacity of 100 Ah (details in Table 2). The methodology of the battery model development, the values of the experimental characterization of the cell, and the electrical and thermal validation of the model are explained in detail in a previous study in the section on battery modelling [27].

Finally, a battery pack with the modeled cell was sized. An arrangement of 160 cells in series and 2 cells in parallel was defined, resulting in a pack with 200 Ah nominal capacity, 512 V nominal voltage and 672 kg mass. As for the thermal part, the battery pack is cooled with glycol–water via a cooling plate system at the bottom of the pack.

2.3. E-machine model

To model the FCEB, models of the powertrain components, such as the traction motor, which is the component with the highest energy demand in a vehicle, are necessary. This bus has two PMSM of 150 kW each. The efficiency maps of these motors are available in the GT-Suite library and are used to estimate their electromechanical behavior. This efficiency map is shown in Fig. 2. From this, the efficiency of the motor can be read as a function of the operating conditions of torque and speed. Fig. 2 also shows that the map contains negative torque values, which means that the electric machine works as a generator under these conditions.

Table 2
Lithim-ion battery main characteristics.

Parameter	Value
Nominal Capacity (Ah)	100
Nominal Voltage (V)	3.2
Chemistry	Lithium iron phosphate (LFP)
Weight (kg)	2.1
Length (mm)	173.9
Width (mm)	28.8
Height (mm)	207.6

2.4. Cabin and HVAC model

Air-conditioning of the vehicle cabin is essential as human comfort is very relevant, especially in mass transport vehicles such as city buses. The energy consumption of the air conditioning system accounts for a significant part of the auxiliary's energy consumption of a vehicle, so for this study, it is necessary to consider cabin and HVAC sub-models in the global FCEB model. Furthermore, it should be mentioned that these subsystems can be thermally integrated with other subsystems, such as the battery or fuel cell, to achieve energy savings.

For the modeled bus, a 60 m^3 cabin with a maximum capacity of 88 passengers was considered. Two heat loads are considered: the heat transmitted through the walls and windows, and the heat generated by the passengers. To calculate the heat transmitted through the walls and windows, it is necessary to know the dimensions, the properties of the materials, the internal temperature of the cabin and the external temperature of the environment. Table 3 shows the dimensions of each component of the cabin. Regarding the heat generated by the passengers, it was established that each passenger generates 100 W of heat due to human metabolism. According to ASHRAE, this value corresponds to the heat generated by an adult at rest [28]. In this study, heat transfer due to solar radiation was not considered, as the simulations are carried out in winter conditions, when solar radiation can be negligible [29].

A compression refrigeration system was considered for air conditioning the cabin. In winter, the system works as a heat pump, with the

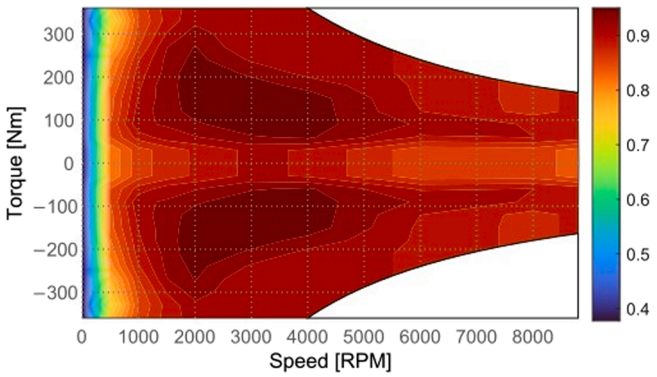

Fig. 2. PMSM efficiency map.

Table 3
Dimensions of the cabin components.

Description	Total Area (m^2)	Thickness (mm)
Roof	30	40
Walls	64	40
Floor	30	40
Windows	10	4

refrigeration circuit operating in reverse thanks to a four-way valve. The bus has four refrigeration circuits operating with R134a refrigerant and each circuit consists of a compressor, an evaporator, an expansion valve, and a condenser. Table 4 lists some characteristics of the components of the HVAC system.

In this study, it was established that the conditioned air was supplied at a rate of 3.5 L/s per passenger, a value within the range of mass flow recommended by ASHRAE for this application [30]. Finally, proportional-integral-derivative (PID) controllers were configured in the HVAC system compressors to regulate their speed to control cabin temperature. A cabin temperature of 19 °C was set as a target for the simulations, which corresponds to a recommended comfort temperature for humans in winter [28]. Fig. 3 shows a schematic diagram of the cabin model in which two main heat transfers are identified: the heat generated by the passengers and the heat transferred by convection through the walls and windows of the bus. The HVAC system combines fresh air with recirculated cabin air and then conditions it to maintain a comfortable temperature inside the bus for the passengers.

2.5. Fuel cell model

For this work, a PEMFC was modelled because this type of fuel cell is the most used in vehicles due to its high energy density and low operating temperatures [31]. The PEMFC is a device that converts the chemical energy resulting from the chemical reaction between oxygen and hydrogen into electrical energy. The output voltage of the PEMFC stack can be expressed as follows [32]:

$$V_{stack} = N_{cell}(V_{OC} - V_{act} - V_{con} - V_{ohm}) \tag{1}$$

Where V_{stack} is the output voltage of the fuel cell stack, N_{cell} is the number of cells in the stack, V_{OC} is the open circuit voltage, V_{act} are the activation losses, V_{con} are the concentration losses and V_{ohm} are the ohmic losses. From Equation (1), the polarization curve of the PEMFC can be estimated.

The activation losses are calculated using the Tafel equation, which is shown in Equation (2).

$$V_{act} = \begin{cases} \frac{R_{gas}T}{2F}\left(\frac{i}{i_0}\right), i \le i_0/(1-\alpha) \\ \frac{R_{gas}T}{2\alpha F}\ln\left(\frac{i}{i_0}\right), i > i_0/(1-\alpha) \end{cases} \tag{2}$$

Where R_{gas} is the universal gas constant, T is the operating temperature of the fuel cell stack, F is the Faraday constant, i is the current density, i_0 is the exchange current density, and α is the charge transfer coefficient. The concentration losses were calculated using Equation (3).

$$V_{con} = -C\ln\left(1 - \frac{i}{i_l}\right) \tag{3}$$

Table 4
Main characteristics of the HVAC system components.

Description	Value
Nominal capacity of each evaporator (kW)	9
Nominal capacity of each condenser (kW)	22
Compressor max speed (rpm)	7000
Compressor displacement (L)	0.028

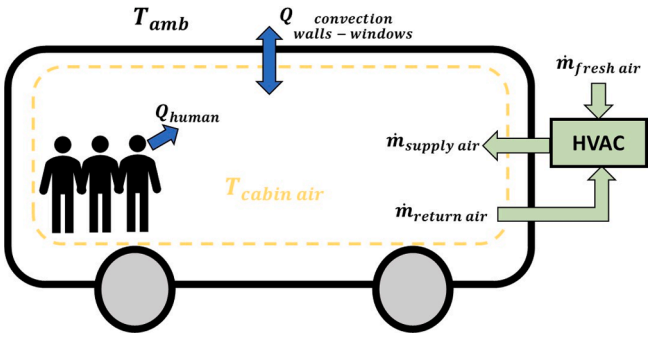

Fig. 3. Cabin model schematic.

Where C is the mass transport loss coefficient and i_l is the limiting current density. Finally, to calculate the ohmic losses or the current losses, it is simply calculated from Ohm's law, being the product of the internal ohmic resistance of the cell and the current.

For this study, a 150 kW nominal power fuel cell was modeled, which was also used in the study by Li et al [33]. Table 5 shows some properties and operating parameters of the PEMFC. To validate the model, the polarization curve estimated by the model was compared with the one determined experimentally in the Li et al. study [33]. Fig. 4 shows both polarization curves and the simulated curve agrees well with the experimental values. The parameters that were adjusted to make the model achieve a polarization curve like the experimental one included the charge transfer coefficient, exchange current density, mass transport loss coefficient, limiting current density, internal ohmic resistance for a single cell, and the open cell voltage loss.

From the polarization curve, the electrical power of the PEMFC can already be read. To calculate the heat power generated by the fuel cell, Equation (4) was used [22].

$$P_{stack,heat} = (N_{cell}V_{OC} - V_{stack})I_{stack} \tag{4}$$

Where $P_{stack,heat}$ is the heat power generated by the PEMFC and I_{stack} is the current of the PEMFC stack.

Regarding the thermal part of the model, the PEMFC stack was considered as a lumped mass that exchanges heat with the fluids and the environment. In Fig. 5, a schematic of a single cell of the modeled stack is shown. The cell is composed of an anode and a cathode, where hydrogen and air flow channels are located, respectively. Catalyst layers and the polymer electrolyte membrane are located between the anode and cathode. Additionally, for each cell there is a cooling plate through which coolant circulates to evacuate the heat generated by the PEMFC. Each of the cells has five channels for each fluid. They are square channels of 1 mm per side and 500 mm in length. To calculate the heat transfer with the fluids, one must know the mass flow rate. In the case of the cathode and anode channels, the mass flow is correlated to the current required by the PEMFC stack, as shown in the Equations (5) and (6) [34].

$$\dot{m}_{H_2} = \frac{I_{stack}N_{cell}}{2F}\lambda_{anode}M_{H_2} \tag{5}$$

Table 5
Operation parameters of the 150 kW PEMFC.

Performance parameters	Value
Nominal operating voltage (V)	568
Nominal operating current (A)	267
Cell number (-)	762
Active surface area (cm^2)	500
Operating temperature (K)	330
Nominal air pressure (bar)	2.06
Nominal hydrogen pressure (bar)	2.24

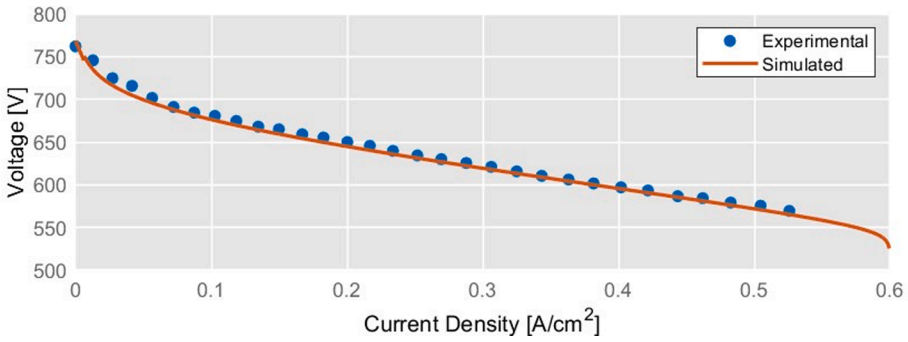

Fig. 4. Polarization curve of the PEMFC stack.

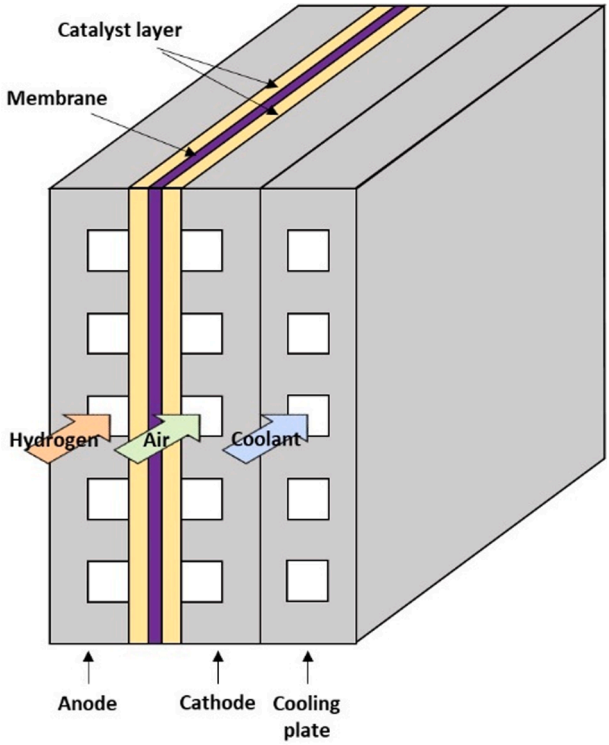

Fig. 5. Schematic diagram of the PEMFC.

$$\dot{m}_{air} = \frac{I_{stack} N_{cell}}{4F x_{O_2}} \lambda_{cathode} M_{air} \tag{6}$$

Where $\dot{m}_{H_2}$ and $\dot{m}_{air}$ are the mass flows of hydrogen and air at the anode and cathode, respectively; F is Faraday's constant; λ is the stoichiometric ratio; M is the molecular weight; and x_{O_2} is the oxygen content in the air. For this study, a value of 3 was set for both λ_{anode} and $\lambda_{cathode}$ as in [35].

To ensure proper operation of the fuel cell system throughout the driving cycle, the model requires various signal conditioning and control systems. To maintain the previously defined stoichiometric ratios, specific control systems were configured. For the air circuit, a controller was set up to sense the current demand of the PEMFC at each moment and regulate the compressor rotational speed accordingly. Similarly, the hydrogen circuit has a controller that considers the recirculation of unreacted hydrogen and adjusts the pump's rotational speed to maintain a hydrogen flow that ensures the established stoichiometric ratio. Also, the mass flow of coolant is controlled with a PID controller that regulates the rotation speed of the pump, maintaining the coolant temperature at the fuel cell outlet at 65 °C. Additionally, the model is equipped with ideal and simple heat exchangers and humidification systems to condition the air at the fuel cell inlet. Finally, the required power signal for the fuel cell is conditioned through moving averages, ensuring a smooth input signal, and avoiding fuel cell response issues.

2.6. Energy management system

The energy available in the system must be managed to meet the vehicle's power requirements and keep the battery sufficiently charged. An energy management strategy was used to control the distribution of energy between the energy sources of the FCEB powertrain. A schematic representation of the FCEB powertrain is shown in Fig. 6. First, the H_2 tanks supplies the fuel cell stack. This fuel cell stack provides power to the high-voltage bus via a unidirectional DC/DC converter. Also, the high-voltage bus DC is connected to the battery pack and the inverter, both bidirectional. The high-voltage bus is unidirectionally connected to all auxiliary units. The auxiliary units consist of compressors for the air conditioning system; fans and blowers that supply air to the evaporators, condensers, and radiators; pumps that circulate fluids in all thermo-hydraulic circuits; and PTC electric heaters that preheat the battery. Finally, the inverter feeds PMSM which are connected to the wheels by means of two gearboxes.

A strategy based on discrete control systems has been proposed for energy management. This control system consists of states and transitions. Each state has a specific output, and the system can only be in one state at a time. Transitions are conditions under which the system changes from one state to another. These conditions are defined using conditional logical statements. Table 6 and Table 7 shows how the energy management system is configured. In the energy management system of the modeled bus, each state defines how much power is requested from the fuel cell. The transition conditions between these states are defined based on several variables: the state of charge of the battery (SOC), the power requested by the FCEB and the maximum discharge power of the battery. This energy management system has five states. The first state is the one with which the system is initialized and is defined as the normal operating state of the fuel cell. The second state is for when the battery reaches a low-level SOC, so that the battery needs to be charged and consequently more power is needed from the fuel cell. The third state has been configured for the scenario where the battery exceeds an already considered high SOC, allowing the vehicle to run on the battery alone, while the fuel cell idle. The fourth state is for when the bus demand is very high and exceeds the maximum discharge power of the battery. Finally, the fifth state is when the vehicle brakes, so the electric machine operates as a generator, putting the fuel cell idling.

2.7. Integral thermal management strategies

The FCEB's vehicle thermal management system consists of the FCTMS, the BTMS, the MTMS and the HVAC system. A schematic diagram of the VTMS base configuration is shown in Fig. 7. The air conditioning circuit uses R134a refrigerant and has a 4-way valve that can be used to change the operating mode for heating or cooling the cabin

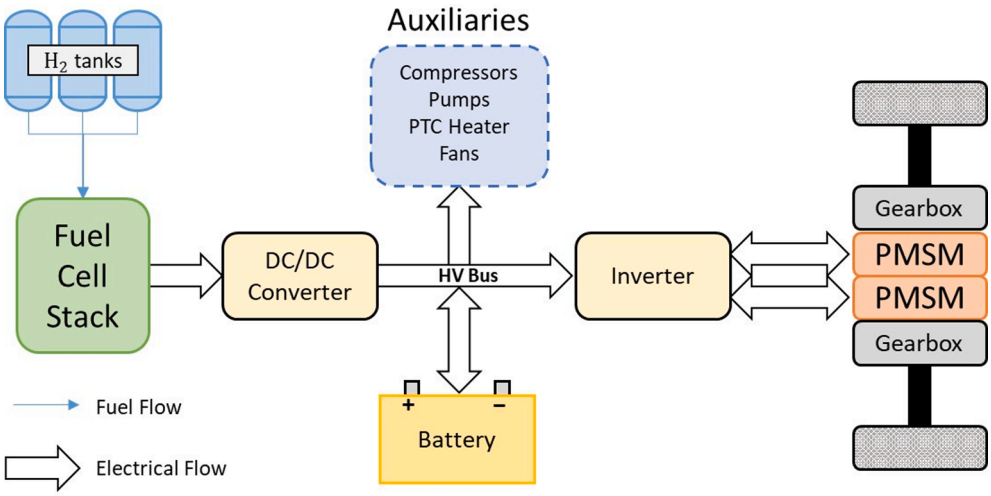

Fig. 6. Schematic of the FCEB powertrain.

Table 6
States of the energy management system.

State N°	State Description	FC Power Request [kW]
1	Normal Operation	20
2	Low SOC, High FC Demand	FCEB Load Request + 20
3	High SOC, FC at idle	4
4	Demands Exceed Normal FC and Battery	FCEB Load Request – Maximum Battery Discharge
5	Regenerative Braking	4

Table 7
Transitions between states of the energy management system.

Transition Description	Transition Conditions	Start States	End States
Battery SOC reaches min limit	Battery SOC <= 30%	1	2
Battery SOC high enough to resume normal operation	Battery SOC > 35%	2	1
Battery SOC reaches max limit	Battery SOC > 70%	1	3
Battery SOC low enough to resume normal operation	Battery SOC <= 65%	3	1
Fuel Cell needs to balance demand	FCEB Load Request > 20 kW + Maximum Battery Discharge	1	4
Battery can balance demand	FCEB Load Request <= 20 kW + Maximum Battery Discharge	4	1
Negative motor torque demand	E-Machine Torque <= 0 Nm	1	5
Positive motor torque demand	E-Machine Torque > 0 Nm	5	1

air. In the four-way valve, when the refrigerant flows through the green lines from point 2 to 3 and from 1 to 4, the system operates as an air conditioner, while when the refrigerant flows through the red lines from point 4 to 3 and from 1 to 2, the system operates as a heat pump. This circuit also has a chiller that exchanges heat with the BTMS circuit to cool the battery when needed. The BTMS circuit circulates 50/50 glycol water and has a three-way valve that diverts the liquid to the chiller or bypasses it as needed. It also has an electric PTC heater that preheats the battery when cold. The FCTMS and MTMS loops are very similar; both circulate 50/50 glycol water and have a radiator and a three-way valve that ensures the coolant circulates through the bypass when system cooling is not required. Finally, the air circuit supplies fresh and recirculated air from the cabin. The air flows through the internal heat exchanger of the air conditioning circuit, which cools or heats the air depending on the operating mode.

The VTMS is crucial in regulating various subsystems by maintaining them within optimal and safe temperature ranges. The FCTMS plays a vital role in keeping the fuel cell system at an ideal temperature between 60 and 80 °C. This temperature range allows the PEMFC to operate efficiently and reduces the risk of drying out the membrane. Similarly, the BTMS is responsible for maintaining the battery pack's temperature between 15 and 30 °C to prevent battery degradation and ensure passenger safety. The MTMS is designed to ensure that the electric machine winding doesn't exceed 120 °C, thereby preventing damage to the winding insulation. Lastly, the HVAC system aims to maintain a comfortable cabin temperature range of 19–21 °C for passengers during winter.

To ensure the subsystems operate within their designated temperature ranges, the VTMS control strategy has been configured using logical threshold control methods and the different modes of operation change depending on the ambient temperature and component temperatures. Fig. 8 shows a diagram of the different modes of operation of the VTMS, where T_{FCcool} is the temperature of the coolant at the output of the fuel cell, $T_{battcool}$ is the temperature of the coolant at the output of the battery, T_{cabin} is the cabin temperature, $T_{motorcool}$ is the temperature of the coolant at the output of the electric machine and T_{batt} is the temperature of the battery. The operating modes of the various thermal management subsystems are mainly divided into heating and cooling. The specific operating modes of each thermal management subsystem are explained in Table 8.

The base configuration is the simplest, where the thermal subsystem of the fuel cell stack is not coupled with other subsystems, so that the heat generated by the fuel cell stack is not used. This configuration is used as a reference for evaluating the other proposed configurations.

To evaluate the benefits that can be obtained by using the residual heat from PEMFC to heat the bus cabin in winter conditions, a VTMS configuration was designed, shown schematically in Fig. 9 and referred to as Configuration 1a in this study. This configuration only has changes in the FCTMS, and air circuits compared to the base configuration. The FCTMS loop has an additional three-way valve and a branch with a radiator located in the cabin air circuit. This new thermostat is configured to circulate the cooling fluid to the cabin radiator if the cabin temperature is below 20 °C. When the cabin temperature reaches 20 °C, it is no longer necessary to continue heating the cabin, so the thermostat begins to close and redirect the coolant to the external radiator. The

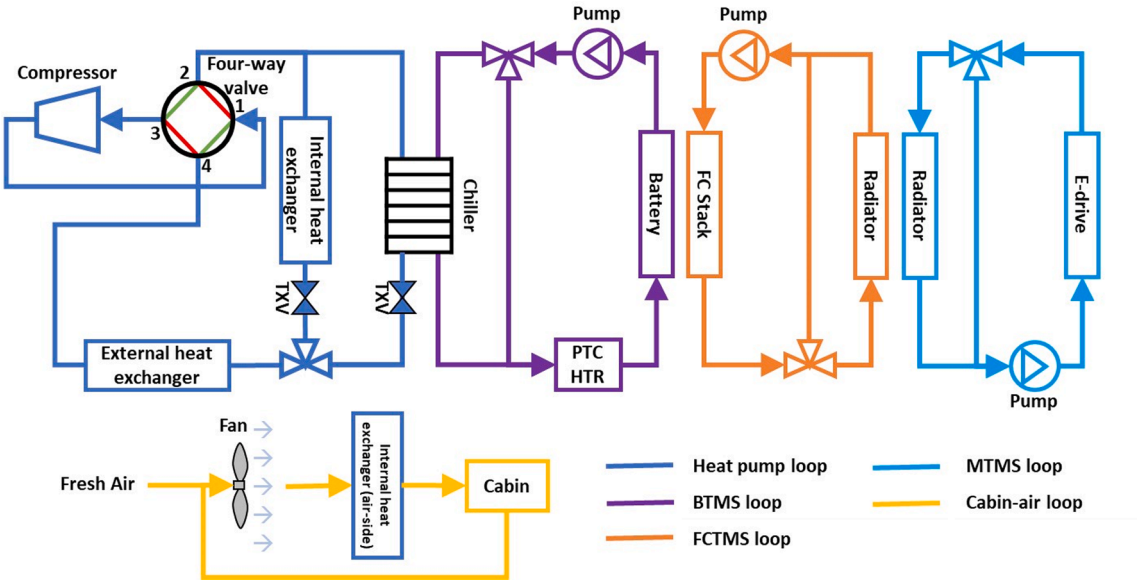

Fig. 7. VTMS diagram: base configuration.

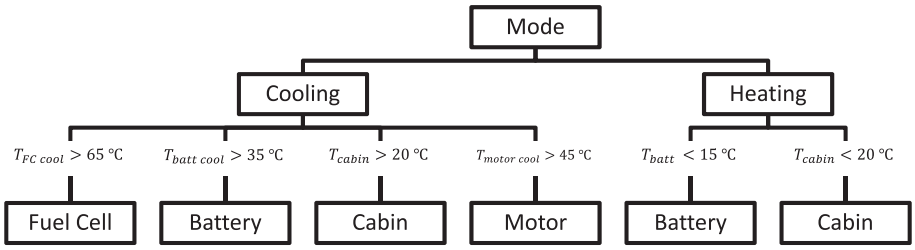

Fig. 8. VTMS control strategy.

Table 8
Operating modes of the VTMS control strategy.

Thermal Management System	Mode	Logical condition	Description
BTMS	Cooling mode	$T_{batt\ cool} >$ 35 °C	The three-way valve directs coolant to chiller
	Bypass mode	$T_{batt\ cool} <$ 28 °C	The three-way valve directs the coolant through the bypass
	Heating mode	$T_{batt} <$ 15 °C	PTC heater on
FCTMS	Cooling mode	$T_{FC\ cool} >$ 65 °C	The three-way valve directs coolant to radiator
	Bypass mode	$T_{FC\ cool} <$ 65 °C	The three-way valve directs the coolant through the bypass
HVAC	Cooling mode	$T_{cabin} >$ 20 °C	4-way valve in Air-conditioning mode. Compressors on
	Heating mode	$T_{cabin} <$ 20 °C	4-way valve in Heat pump mode. Compressors on
MTMS	Cooling mode	$T_{motor\ cool} >$ 45 °C	The three-way valve directs coolant to radiator
	Bypass mode	$T_{motor\ cool} <$ 35 °C	The three-way valve directs the coolant through the bypass

FCTMS radiator was placed directly behind the blower in the air circuit. A thermostat was installed that bypassed the heat pump system's heat exchanger when the air temperature at the outlet of the first radiator exceeded 35 °C. This was done for two reasons: first, so that the heat pump system would work properly; and second, to avoid comfort problems caused by an excessively high air inlet temperature into the cabin.

Furthermore, this configuration was slightly modified to prioritize cabin heating rather than fuel cell preheating. This was done by simply changing the location of the valves and branches so that the coolant first circulates through the cabin radiator until the cabin air reaches the target temperature, then bypasses the radiators so that the fuel cell reaches the optimum operating temperature, and finally, when both temperatures are reached, the heat is dissipated to the environment via the external radiator. This configuration is referred to as Configuration 1b.

Another configuration has also been proposed to evaluate the benefits of using the waste heat from the fuel cell to preheat the battery. This proposal is referred to as Configuration 2 and is shown in Fig. 10. This configuration is intended to operate under winter conditions. The change from the base configuration was that the BTMS loop was eliminated, and the battery cooling plate was included in the FCTMS loop. A thermostat was also used for this purpose. When the battery reaches a temperature of 15 °C, the thermostat begins to close and directs the coolant to the radiator, which releases the heat to the environment.

Finally, a VTMS was defined to use the heat from the fuel cell to heat the cabin and the battery. For this purpose, the modifications made in Configuration 1 and Configuration 2 were combined. This VTMS was designated as Configuration 3 and is shown schematically in Fig. 11.

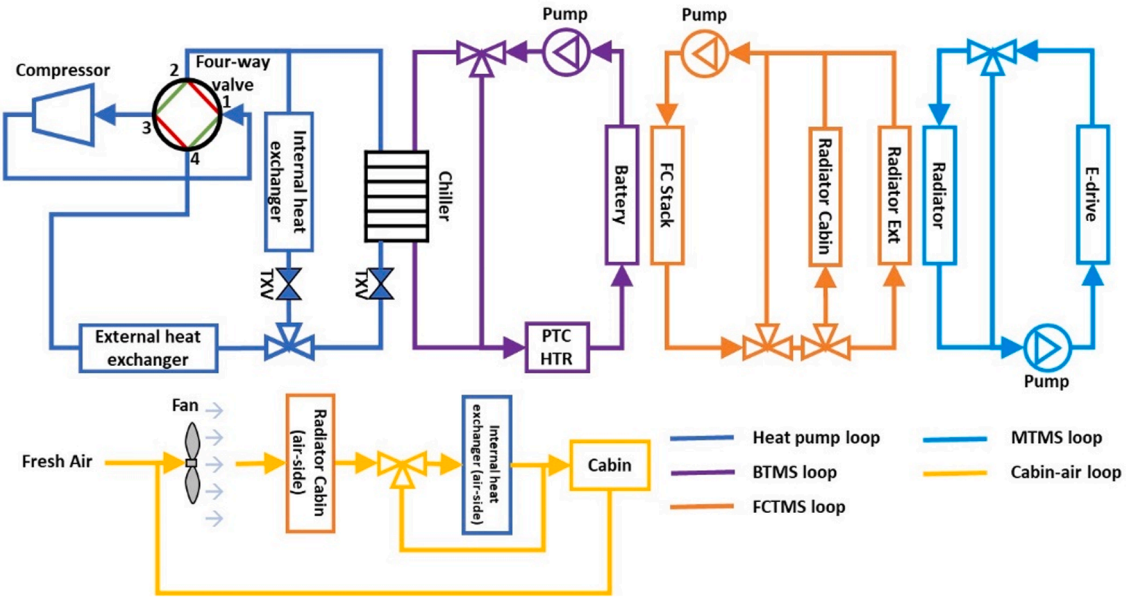

Fig. 9. VTMS diagram: Configuration 1.

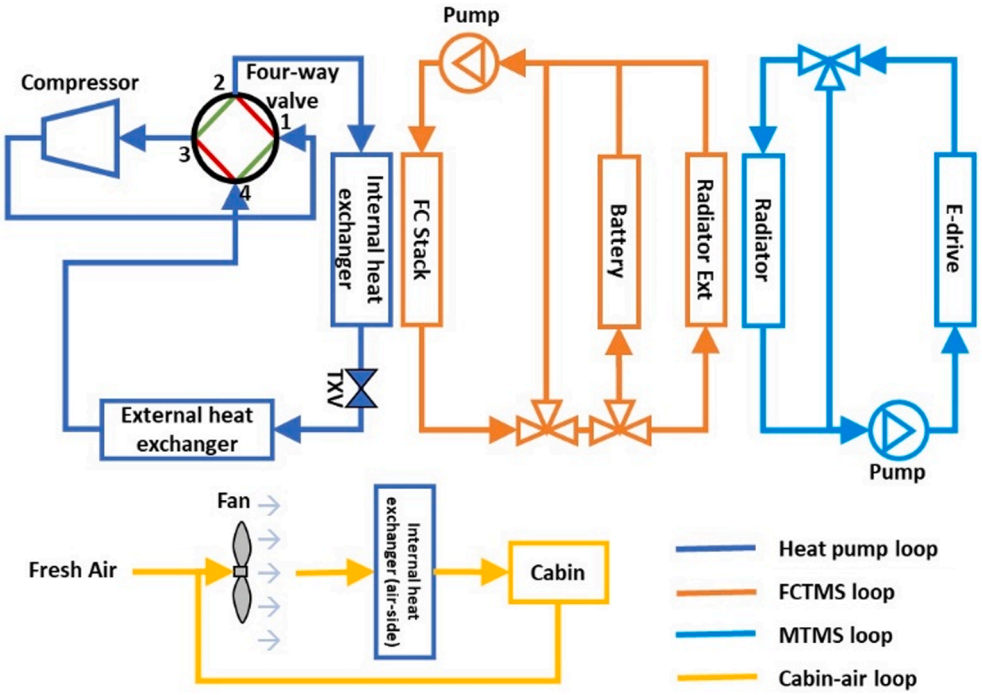

Fig. 10. VTMS diagram: Configuration 2.

2.8. Driving cycles and operating conditions

To evaluate the various VTMS configurations, the model simulations were carried out under operating conditions that were as realistic as possible. To isolate the impact of the various proposed VTMS and ensure comparability, all simulations were carried out under the same operating conditions. Various factors, such as driving style, ambient temperature, terrain, vehicle weight, and payload, can affect vehicle performance and, consequently, the cruising range. All these factors were standardized for all simulations.

For this purpose, a driving cycle corresponding to one of the routes used by the bus fleet of the Valencia Municipal Transport Company (EMT) was specified. EMT provided the data for the driving cycle of line 18. Fig. 12 shows the route of line 18 and the speed profile of the bus travelling this route for five and a half hours. This is a typical driving cycle for city buses, never exceeding 60 km/h, with many stops due to city traffic and stops for passengers to get on and off.

As mentioned above, all simulations were carried out under winter conditions, as we want to evaluate the benefits of using the residual heat of the fuel cell to preheat other components of the FCEB. For this reason, an ambient and initialization temperature of 5 °C for all components was set in all simulations, as this is a typical temperature in Valencia, Spain, in winter. Also, in all simulations it was assumed that the bus has half of the maximum allowed passenger capacity during the whole journey. Finally, the simulations were performed with three different battery initial states of charge of charge to evaluate all VTMS configurations in

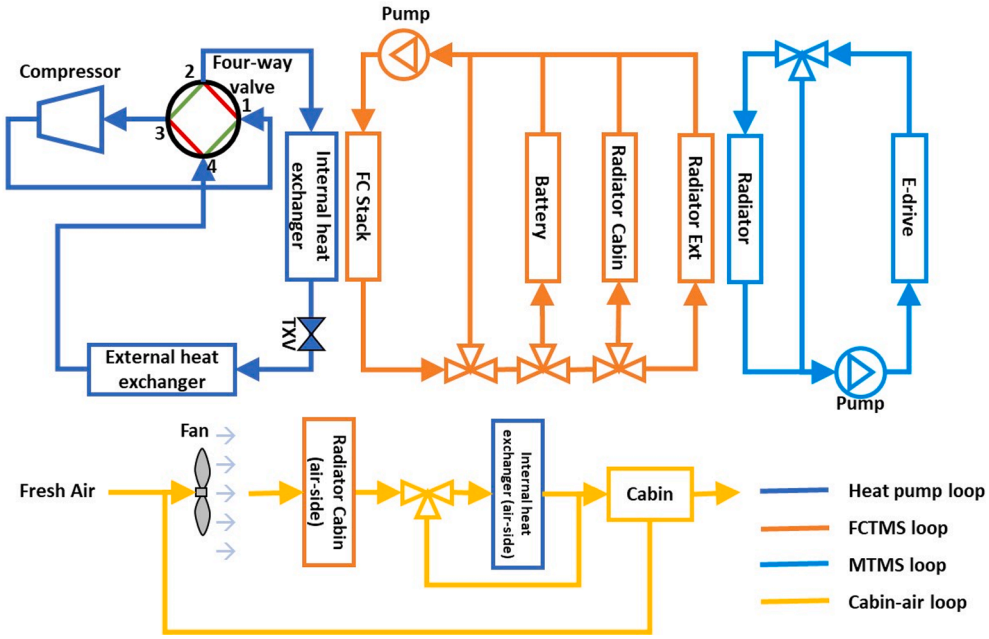

Fig. 11. VTMS diagram: Configuration 3.

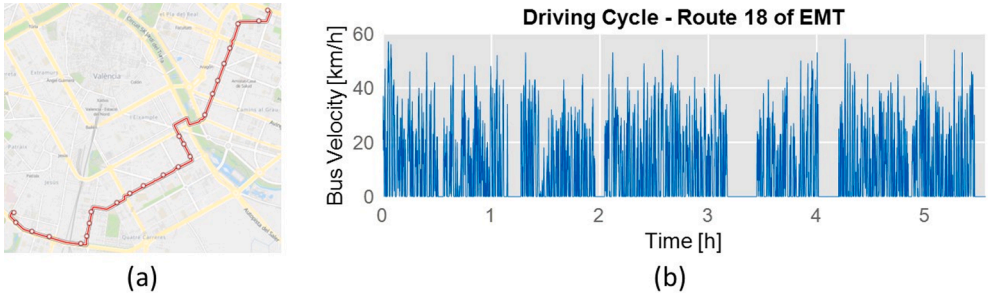

Fig. 12. Real driving cycle: (a) route 18 trajectory and (b) speed profile of the bus.

different states of the energy management system to account for different performance requirements of the fuel cell. These initial states of charge were 20%, 50% and 90%0.3.1.

3. Results

3.1. Distribution of bus energy consumption during a driving cycle

To evaluate the potential advantages of VTMS proposals, it is important to understand the limitations of the system, and where and when actions can be taken to achieve greater benefits. For this reason, an initial assessment of the base configuration was conducted to

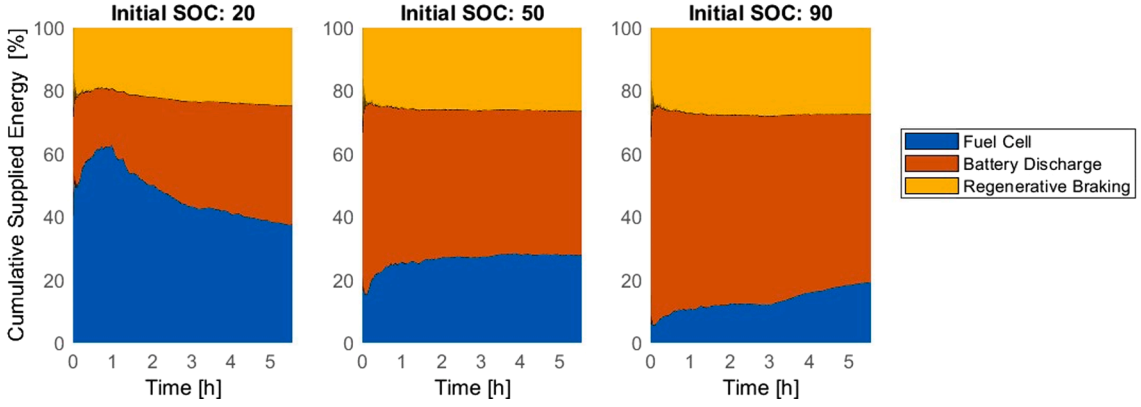

Fig. 13. Percentage distribution of accumulated energy supplied with the baseline VTMS configuration.

understand how energy is distributed in the FCEB throughout the driving cycle. Fig. 13 and Fig. 14 show the cumulative energy delivered and consumed throughout the FCEB driving cycle with the baseline VTMS configuration, respectively. Fig. 13 shows that the supplied energy is divided among three energy sources: the fuel cell, the battery (when is discharging), and the regenerative brake. It can also be seen that the lower the initial SOC, the higher the percentage of energy supplied by the fuel cell. This is since the energy management system is configured to request more power from the fuel cell when the SOC is low. Observing this, it can be intuited that in these conditions where the fuel cell is in most demand, it will be possible to take more advantage of the residual heat of the fuel cell.

The analysis of Fig. 14 shows that when the initial SOC is 20% at the beginning of the driving cycle, the energy spent on charging the battery is greater than in the other cases. This is also due to the energy management strategy. At the beginning of the cycle, the fuel cell takes over most of the energy consumption of the bus and charges the battery. Another critical aspect is the consumption by the auxiliary units during the driving cycle. In all cases, the energy consumption by the auxiliaries after the driving cycle accounts for about 8% of the total electrical energy consumption. In addition, in all cases there is a significant peak in the consumption by the auxiliaries at the beginning of the drive cycle. This peak is because the vehicle's components are cold at the beginning and need to reach their optimum operating temperature as quickly as possible, so elements such as electric heaters and compressors operate at higher power.

Fig. 15 shows the distribution of accumulated consumed energy of the auxiliary components during the driving cycle. At the beginning of the simulation, the battery PTC heater consumes up to 80% of the energy consumed by the auxiliary components. This is because the battery must reach the optimal operating temperature of 15 °C quickly to avoid performance degradation and deterioration. Another aspect to consider is the consumption by the compressors, which represents almost 45% of the total consumption of the auxiliary units. It is important to highlight the consumption of these two components, since the proposed VTMS configurations aim to reduce the consumption of these auxiliary components.

3.2. Utilization of the heat dissipated by the fuel cell to heat cabin

Fig. 16 shows a multivariate comparison between the base configuration and Configurations 1a and 1b for the three initial SOC conditions. In the results for an initial SOC of 20%, it can be observed that at the end of the driving cycle the battery has a higher state of charge with Configuration 1b than with Configuration 1a and even more than with the base configuration. This SOC behavior is explained by observing the consumption of the HVAC system compressors. In Configuration 1b, the compressors are used very little only at the beginning of the run. Since this configuration focuses on heating the cabin with the waste heat from the fuel cell, the heat pump system is practically superfluous. Something similar happens in Configuration 1a. However, in this configuration the fuel cell is preheated first, so at some moments the support of the heat pump system is needed to heat the cabin. When analyzing the hydrogen consumption curves, there is a slight variation between the curves, with the curve corresponding to the base configuration clearly predominating. This is because in the other configurations, due to the greater energy savings, a state of charge of 35% is reached earlier, at which point there is a change of state in the energy management system, which changes the power requirement of the fuel cell. A similar analysis can be performed for the 90% initial SOC condition, with analogous behaviors and conclusions. In conclusion, utilizing the waste heat generated by the fuel cell to heat the compartment can reduce the need for HVAC system compressors, resulting in higher battery state of charge and ultimately saving hydrogen consumption at the end of the driving cycle.

Fig. 17 shows the cabin and fuel cell temperature curves for each configuration. When analyzing the fuel cell temperatures, the first thing to note is that the curve for Configuration 1b deviates the most and has lower temperatures than the other two curves for almost the entire driving cycle. With this type of fuel cell, it is ideal that they operate at temperatures between 60 °C and 80 °C and are therefore in a safe range where they are more efficient. The effect of the fuel cell efficiency can be better understood by looking at the hydrogen consumption in the initial SOC condition of 50% (Fig. 16), since in this case the energy management system works identically in all configurations. The hydrogen consumption is slightly higher in Configuration 1b, as the fuel cell operates at a lower efficiency. However, it seems that operating the fuel cell at a lower temperature, the increase in hydrogen consumption is not so relevant.

The temperature curves of the cabins in Fig. 17, show that they are correctly maintained at the target temperature in all cases and configurations. It can also be seen that the time of reaching the target temperature coincides with the decrease in compressor power. Furthermore, in the case of an initial SOC of 20%, the target temperature is reached faster with Configurations 1a and 1b, which is advantageous. This is because at this initial condition the power demand of the cell is higher and therefore the heat generated is also higher.

3.3. Utilization of the heat dissipated by the fuel cell to heat battery

Fig. 18 shows the SOC and hydrogen consumption curves during the driving cycle for Configuration 2 and the baseline. For all the initial conditions of SOC, it can be observed that energy savings are achieved with Configuration 2, both for SOC and hydrogen consumption. The energy saving is due to the fact that Configuration 2 does not use an electric PTC heater to heat the battery but uses the waste heat from the fuel cell for this purpose. From an energy perspective, Configuration 2 is

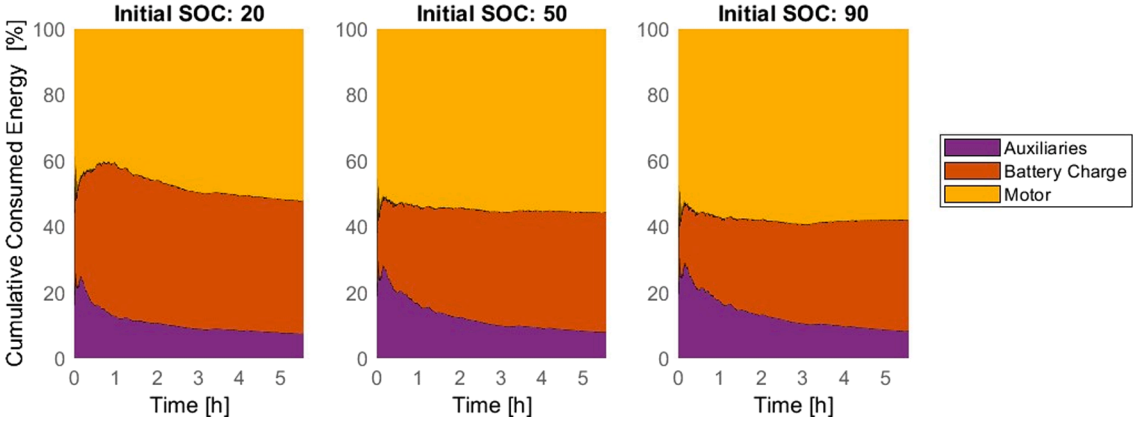

Fig. 14. Percentage distribution of accumulated energy consumed with the baseline VTMS configuration.

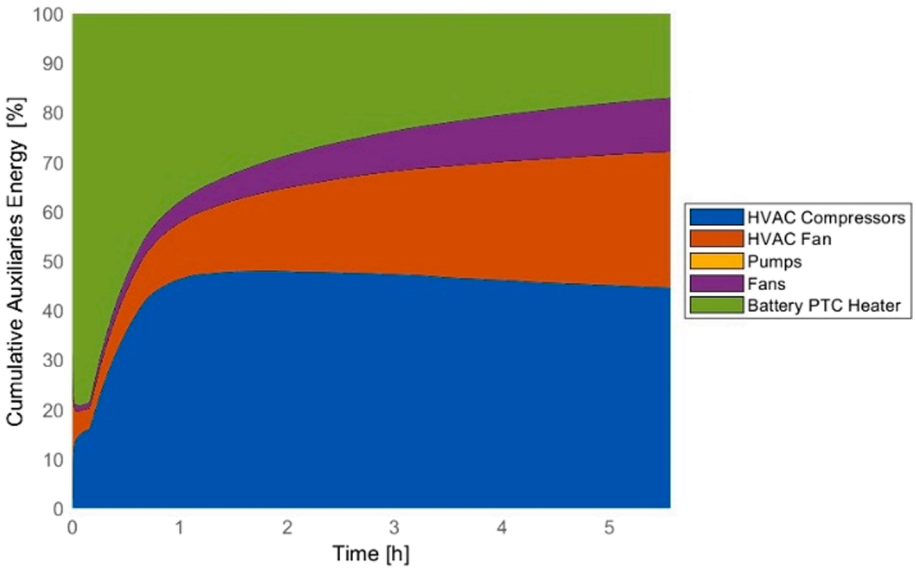

Fig. 15. Percentage distribution of accumulated energy consumed by auxiliary units with the baseline configuration.

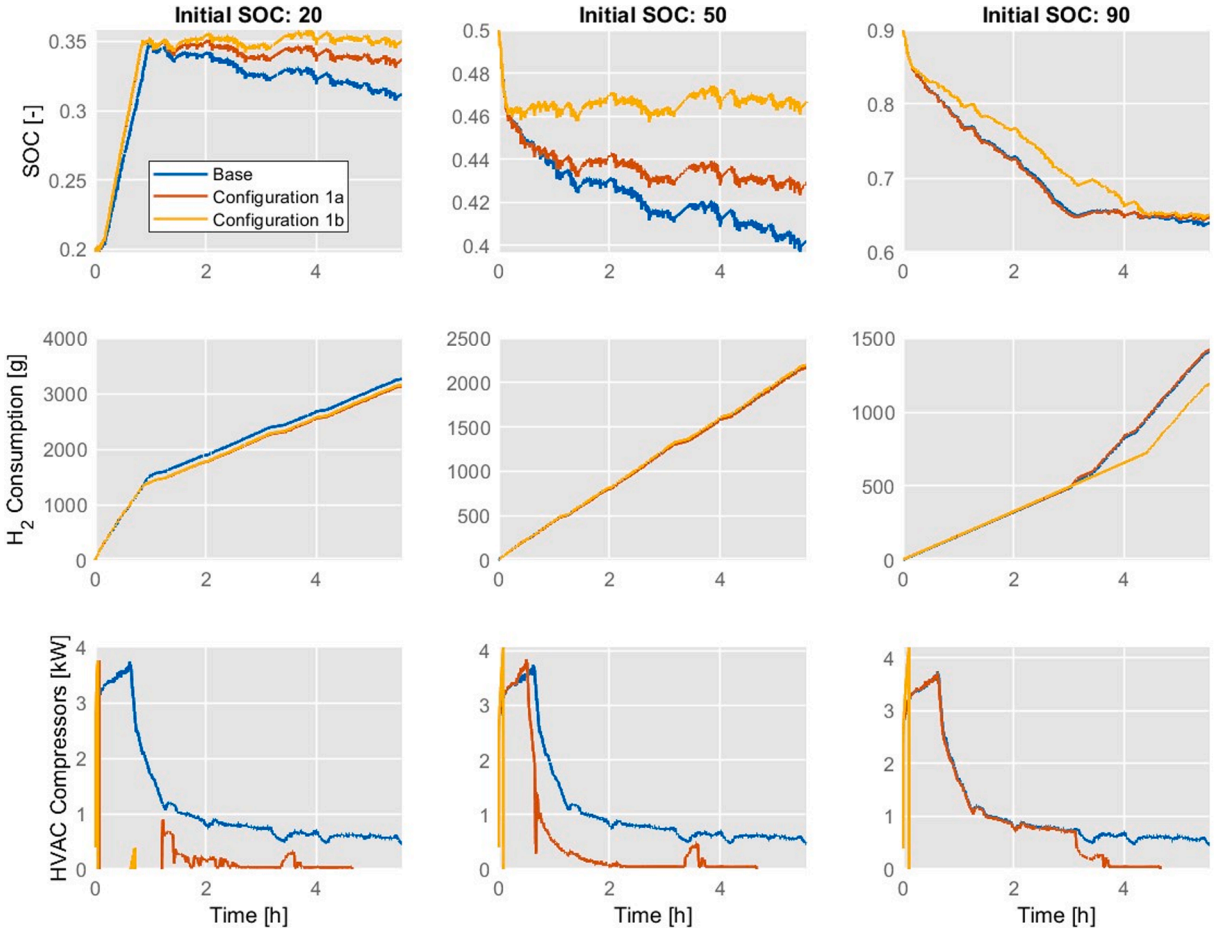

Fig. 16. Comparison among base configuration; Configuration 1a; and 1b: battery SOC, hydrogen consumption, and compressor power throughout the driving cycle.

more advantageous than the base configuration. However, it would have to be checked how the battery preheats and whether it reaches its optimal operating temperature in a reasonable time.

Fig. 19 shows the temperature curves of the fuel cell and the battery for both configurations, the base and Configuration 2. For the initial condition of 20% SOC, the temperature curves are almost identical, so battery heating is considered appropriate, as the battery must operate in optimal operating ranges as quickly as possible. However, battery heating occurs more slowly for the other two initial SOC conditions. This is so because, for these initial SOC conditions, the power demand on the fuel cell stack is lower, especially in the case of an initial SOC of 90%. Looking at these results, it can be concluded that Configuration 2 is only

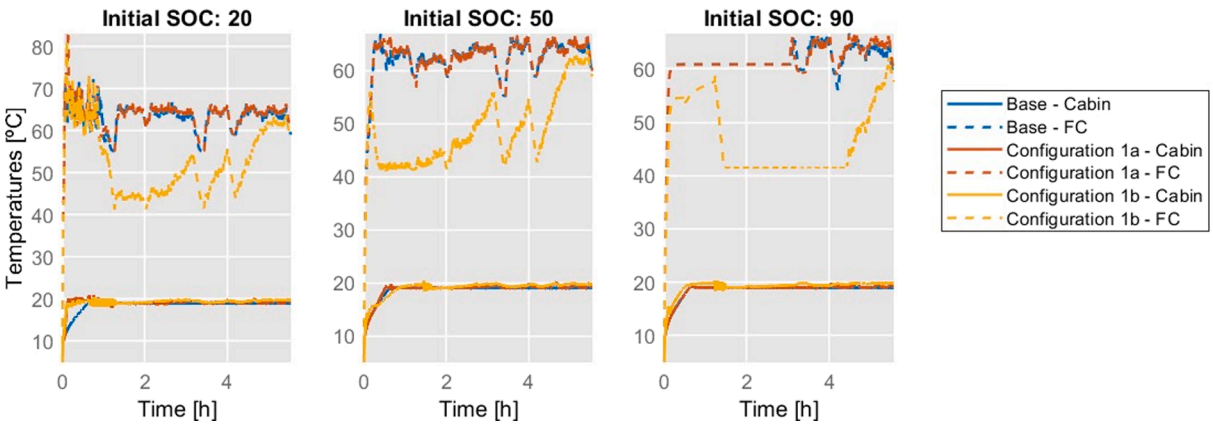

Fig. 17. Comparison among base configuration; Configuration 1a; and 1b: cabin and fuel cell stack temperatures throughout the driving cycle.

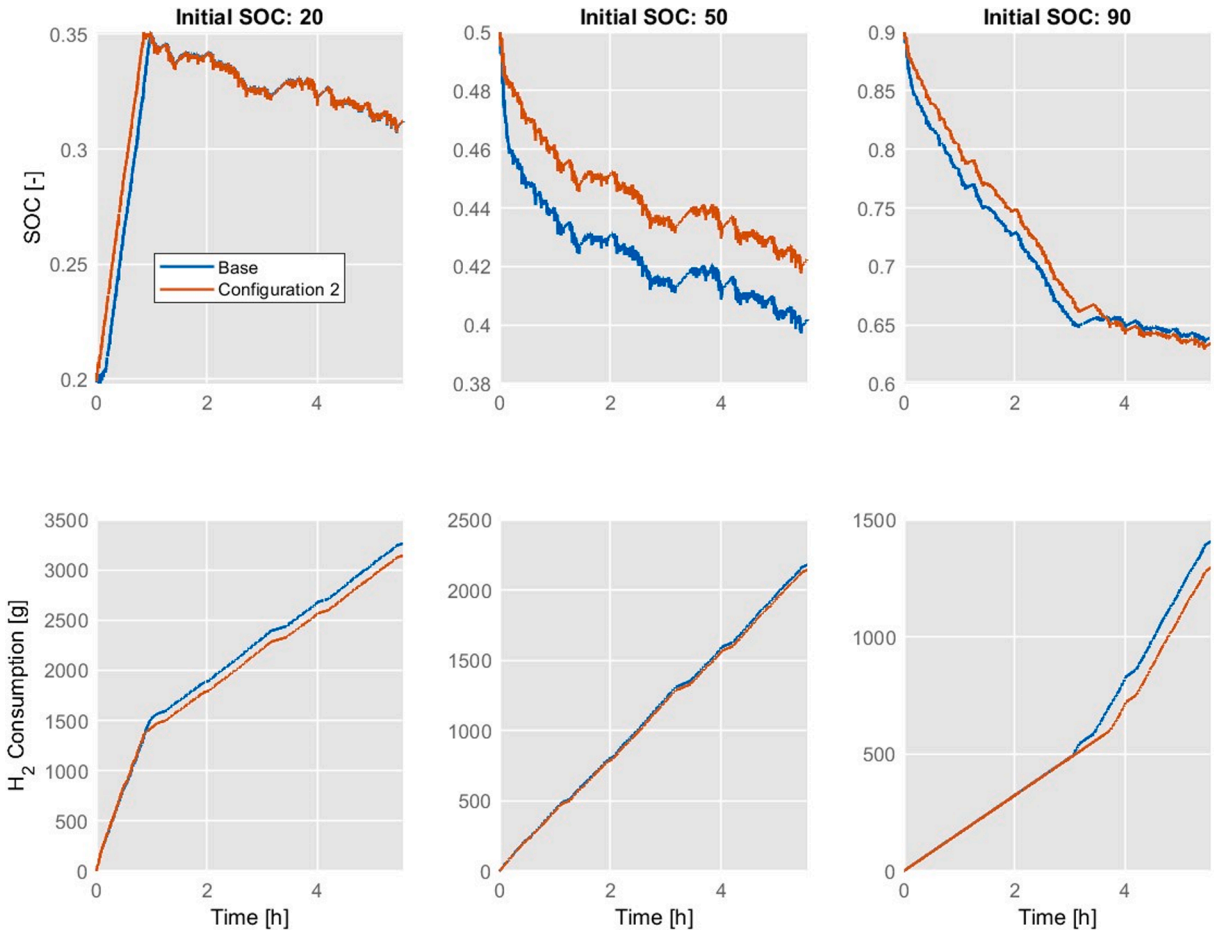

Fig. 18. Comparison among base configuration and Configuration 2: battery SOC and hydrogen consumption throughout the driving cycle.

appropriate if the demand for the fuel cell is high enough so that the waste heat is sufficient to heat the battery rapidly. Even though energy savings can be achieved, the risk of operating the battery at low temperatures and thus accelerating its degradation can make this configuration detrimental to the FCEB.

3.4. Hybrid configuration case

The last configuration evaluated was Configuration 3, which is a combination of the proposed configurations. Fig. 20 shows the SOC curves, the hydrogen consumption, and the consumption of the heat pump system compressors over time. After a similar analysis to the previous results, Configuration 3 shows savings for all the initial conditions of SOC, either in SOC or in hydrogen consumption. As with Configuration 2, this proposal does not use the battery's PTC heater, so the system saves the energy invested in this component. As soon as the battery exceeds a temperature of 15 °C, the residual heat is used to heat the cabin. This becomes clear when looking at the power curves of the compressor in Fig. 20 and the temperature curves in Fig. 21. In the three initial conditions, when both the fuel cell and battery temperatures reach a temperature threshold of 65 °C and 15 °C, respectively, the power of the compressors drops abruptly since, at this moment, the

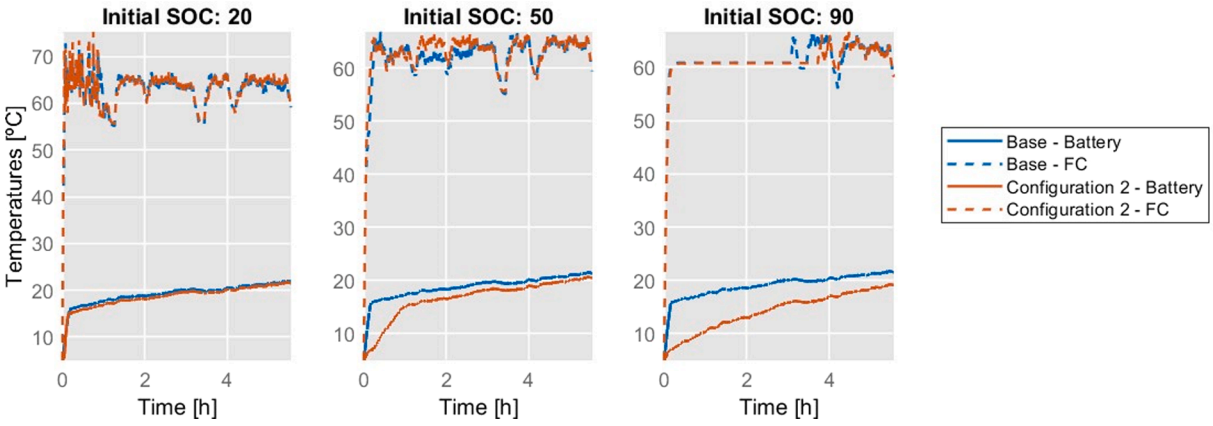

Fig. 19. Comparison among base configuration and Configuration 2: battery and fuel cell stack temperatures throughout the driving cycle.

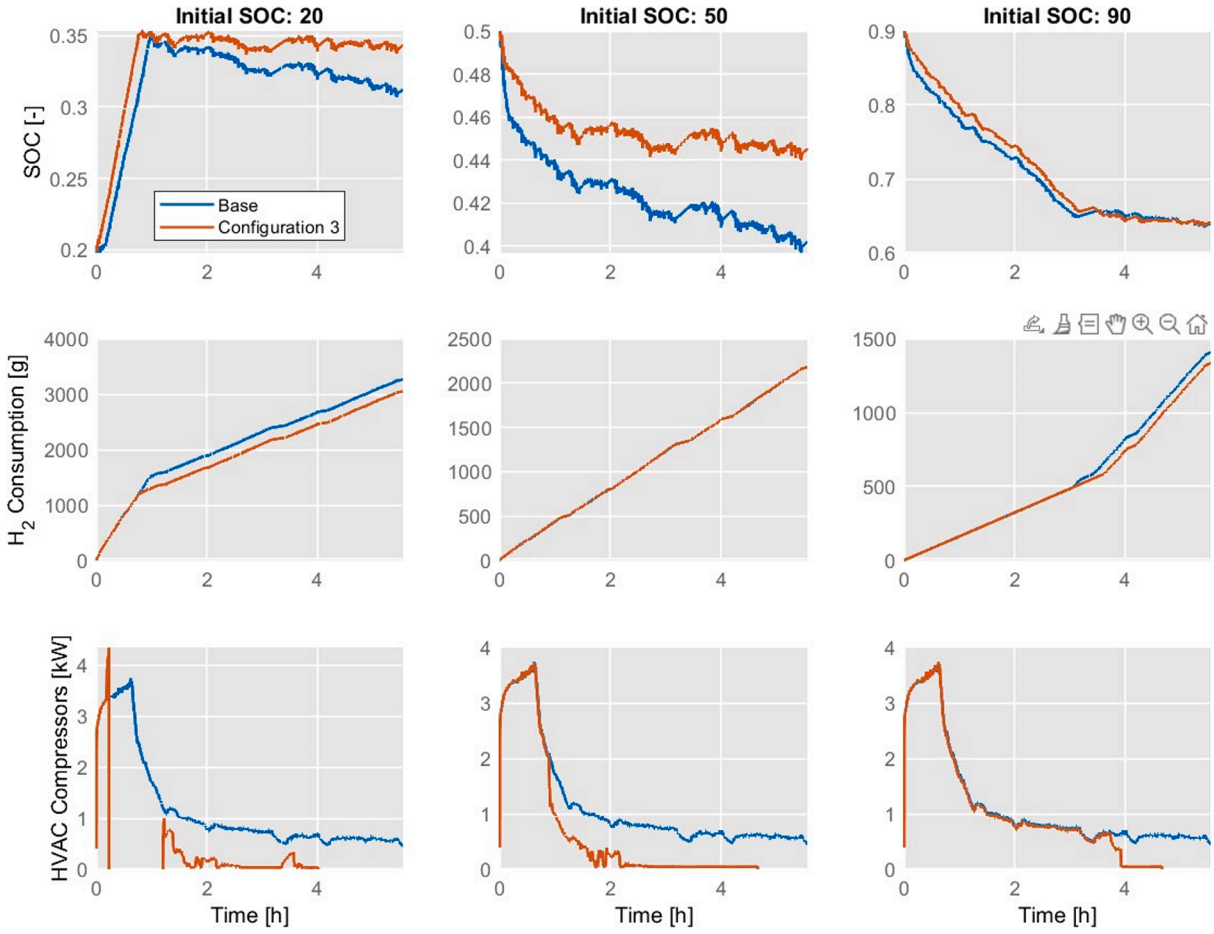

Fig. 20. Comparison among base configuration and Configuration 3: battery SOC, hydrogen consumption, and compressor power throughout the driving cycle.

cabin is heated by the heat fuel cell residual.

This configuration also has the same problem as Configuration 2 regarding the rate at which the battery heats up. Only in the case of an initial SOC of 20% is the optimum temperature reached quickly. Despite the additional savings in compressor consumption, it is not advisable to damage the battery by operating at low temperatures for long periods. One solution could be to propose a control strategy that regulates a PTC heater based on the residual heat of the fuel cell, ensuring rapid pre-heating of the battery.

3.5. Summary of results

Finally, a quantitative comparison of the different proposed VTMS configurations was performed. This comparison was done by comparing the SOC and the fuel consumption at the end of the driving cycle. In order to standardize the energy consumption of the fuel cell and the battery, the energy consumption was calculated according to Equation (7).

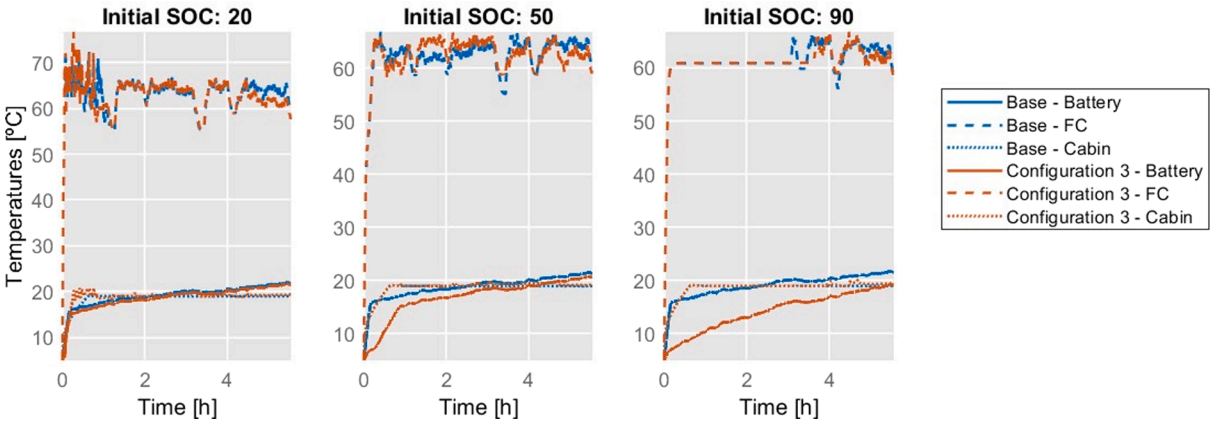

Fig. 21. Comparison among base configuration and Configuration 3: battery, cabin, and fuel cell stack temperatures throughout the driving cycle.

$$EnergyConsumption = \int_0^{t_f} P_{batt} \bullet dt + LHV_{H_2} \bullet m_{H_2} \quad (7)$$

Where P_{batt} is the instantaneous power of the battery, t_f is the duration of the driving cycle, LHV_{H_2} is the lower heating value of hydrogen, and m_{H_2} is the mass of hydrogen consumed throughout the entire journey. This parameter will be used to globally evaluate the energy savings between the different configurations.

Fig. 22 shows the final SOC of the battery for all configurations and the three initial SOC conditions. It can be observed that Configuration 1b completes the cycle with the highest SOC in all cases, reaching SOC differences of more than 6% compared to the baseline configuration.

Fig. 23 shows hydrogen consumption for all configurations. For the initial condition of 20% SOC, Configuration 3 was the one that achieved the greatest hydrogen savings, with a savings of 6.6% compared to the baseline configuration. For the initial condition of 50% SOC, further hydrogen savings were achieved with Configuration 2, with a savings of 1.7% compared to the base configuration. Finally, for the case with an initial SOC of 90%, further savings were achieved with Configuration 1b, with a savings of 15.6% more hydrogen than the baseline configuration.

The final comparison is shown in Fig. 24, where the estimated energy consumed is plotted. For the initial condition of 20% SOC, the most savings were achieved with Configuration 3, with savings of 10.1% for the base configuration. For the other two initial conditions of 50% and 90% SOC, more significant savings were achieved with Configuration 1b, 7% and 10.6%, respectively, compared to the baseline configuration. Analysis of this comparison suggests that for initial conditions where the fuel cell is operating at high power, a VTMS with Configuration 3 is more advisable, as much residual heat from the fuel cell is available to quickly heat the cabin and battery. For other operating conditions, a VTMS with configuration 1b would be advisable, which primarily heats the cabin. Although the fuel cell does not operate in the temperature ranges where it is most efficient, the overall energy savings with this VTMS is still remarkable.

In summary, using the different proposed VTMS provides advantages in terms of overall energy consumption savings of the vehicle compared to the base configuration, regardless of the initial SOC condition. In operating conditions where the fuel cell system has high demand (initial SOC 20%) and thus generates a greater amount of heat, the most convenient strategy is to utilize residual heat to preheat the battery and cabin. However, this strategy may be disadvantageous in operating conditions where the fuel cell system is not as demanding since there may not be enough residual heat available to quickly heat the battery to its optimal temperature range and then condition the cabin.

For medium and low fuel cell demand conditions (initial SOC 50% and 90%), the most advantageous strategy is to use the residual heat from the fuel cell system to heat the cabin, with the control strategy prioritizing achieving the optimal cabin temperature. This way, the greatest overall energy savings for the simulated driving cycle can be achieved. However, it should be noted that with this VTMS strategy, the PEMFC system may not be operating within optimal temperature ranges for this type of fuel cell, which could impact its efficiency. Additionally, not carefully controlling the temperature of the fuel cell could affect its degradation and lifespan, which could be disadvantageous.

4. Conclusions

In this work, a global model of a fuel cell electric bus was developed. Based on this model, different VTMS strategies were evaluated that use

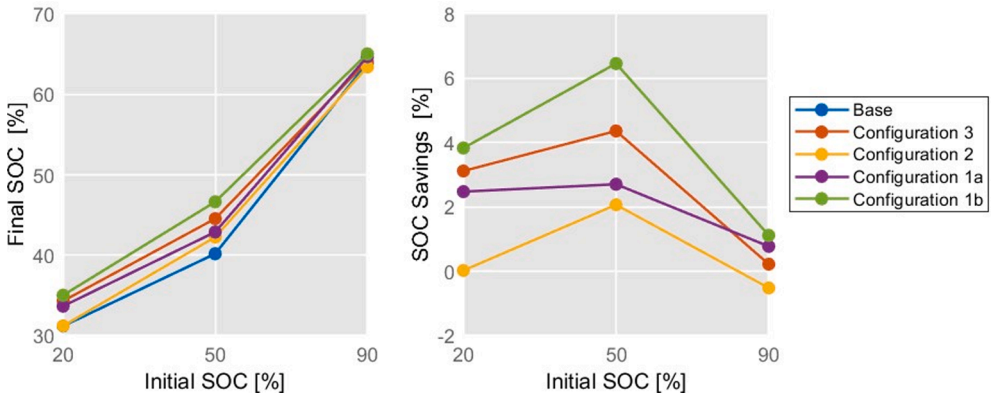

Fig. 22. Battery SOC at the end of the driving cycle for each case and VTMS configuration.

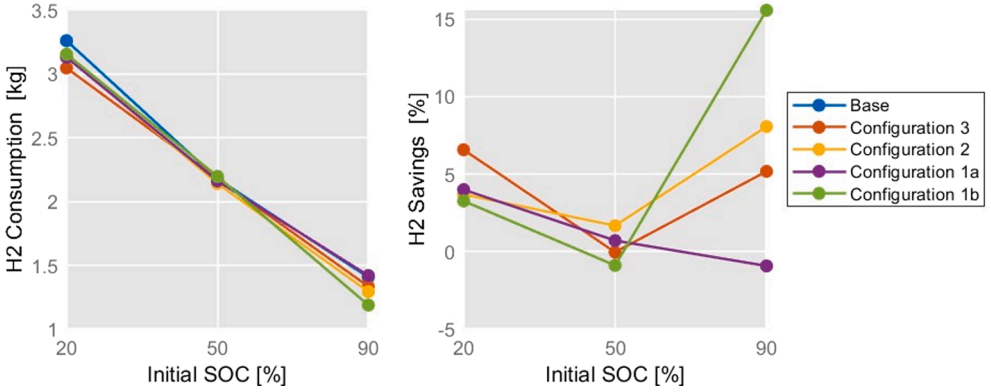

Fig. 23. Hydrogen consumption for each case and VTMS configuration.

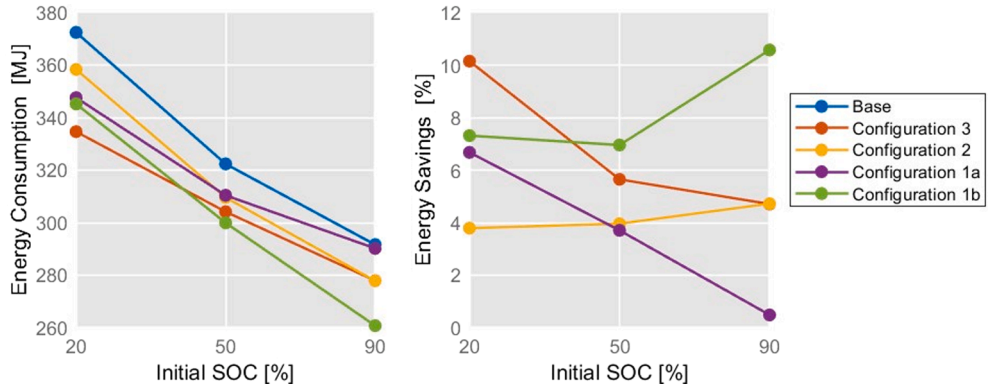

Fig. 24. Energy consumption for each case and VTMS configuration.

the residual heat of the fuel cell for winter conditions in Valencia. Four VTMS configurations, including the base configuration, were defined to perform this assessment. These configurations were designed to use the waste heat from the fuel cell to heat the cabin, the battery or both. The assessment was carried out by simulating a driving cycle of the bus fleet of the public transport company of Valencia, Spain (EMT). All simulations were carried out for winter weather conditions. From the results obtained, the following can be concluded:

- The energy management system of the FCEB plays a crucial role in the VTMS, as the power drawn from the fuel cell and thus the available residual heat depends on it. Higher power consumes more fuel, but also generates more heat, which can help to reduce the consumption of other components of the vehicle.
- The energy consumption of the auxiliary components accounts for up to 8% of the total consumption of the FCEB during the entire drive cycle in the basic configuration of the VTMS. Of this auxiliary component consumption, electric heaters and compressors account for about 60%. It is important to highlight this, as thermal management strategies can reduce the consumption of these auxiliary components and thus achieve valuable energy savings.
- At the beginning of the driving cycle, the power demand of the auxiliaries is higher because the different components of the vehicle must reach an optimal operating temperature. It would be interesting to develop energy management strategies with more precise and complex control so that the fuel cell operates at high demand during this phase, when all components are cold, to make better use of its residual heat.
- With the VTMS configuration that uses the residual heat from the PEMFC to heat the cabin, savings were achieved in the consumption of the compressors of the heat pump system. In addition, the temperature in the cabin could be maintained at the target temperature. Although the fuel cell stack does not operate in the temperature ranges where it is most efficient, a VTMS that prioritizes heating the cabin achieves more significant savings in compressor consumption.
- Significant energy savings can be achieved using the PEMFC waste heat to preheat de battery, but it is important to assess how quickly the battery heats up with this setting. Ideally, this configuration would only be used when the demand for the PEMFC stack is very high at the beginning of the drive cycle. Thus, a large amount of residual heat is available to preheat the battery and reach an optimal operating temperature range.
- It is also an interesting alternative to consider a hybrid configuration that uses the residual heat from the fuel cell to heat the interior and the battery when needed. Although such a VTMS is more complex and requires more sophisticated control, this configuration can be very beneficial. The fuel cell in this type of vehicle generates so much heat that it can heat multiple systems simultaneously.
- For the initial SOC condition of 20%, the highest energy savings were achieved with Configuration 3, which saved 10.1% energy compared to the baseline configuration. For the other two initial conditions, 50% and 90% SOC, more significant savings of 7% and 10.6% respectively were achieved with Configuration 1b compared to the base configuration.

There are also some limitations to thermal management strategies proposed. Firstly, the implementation of these strategies can increase the complexity and cost of the system. Secondly, certain strategies may require additional components, such as heat exchangers, which can add to the weight and volume of the system. Thirdly, there may be limitations in the ability to recover waste heat, especially if the temperature

difference is not significant enough to justify the use of additional equipment. Additionally, there may be limitations on the use of residual heat in certain operating conditions, such as during high power demand or low ambient temperatures, which can result in inadequate heating for the cabin or battery preheating.

After this study, it can be concluded that the VTMS system is of great importance as significant energy savings can be achieved for different operating conditions. In future work on this topic, the VTMS can be considered with more detailed and complex control systems that can manage the available heat generated by the different elements according to operating conditions and system requirements.

Funding

This work was supported by Generalitat Valenciana within the framework of the PROMETEO 2020 project "Contribution to the decarbonization of transport by optimizing the thermal management of vehicle batteries electrified" with reference number PROMETEO/2020/042.

CRediT authorship contribution statement

Alberto Broatch: Conceptualization, Methodology. **Pablo Olmeda:** Supervision, Methodology, Writing – review & editing. **Xandra Margot:** Project administration, Visualization. **Sebastián Aceros:** Investigation, Software, Validation, Writing – original draft.

Declaration of Competing Interest

The authors declare that they have no known competing financial interests or personal relationships that could have appeared to influence the work reported in this paper.

Data availability

The data that has been used is confidential.

Acknowledgments

The authors gratefully acknowledge the support of EMT Valencia for providing the driving cycles of its fleet on routes 18.

References

[1] Zhang R, Fujimori S. The role of transport electrification in global climate change mitigation scenarios. Environ Res Lett 2020:15. https://doi.org/10.1088/1748-9326/ab6658.
[2] Perdiguero J, Jiménez JL. Policy options for the promotion of electric vehicles : a review. IREA- Work Pap 2012;IR12/08:1–44.
[3] Wang N, Pan H, Zheng W. Assessment of the incentives on electric vehicle promotion in China. Transp Res Part A Policy Pract 2017;101:177–89. https://doi.org/10.1016/j.tra.2017.04.037.
[4] Wang N, Tang L, Pan H. A global comparison and assessment of incentive policy on electric vehicle promotion. Sustain Cities Soc 2019;44:597–603. https://doi.org/10.1016/j.scs.2018.10.024.
[5] Suarez C, Martinez W. Fast and ultra-fast charging for battery electric vehicles - a review. In: 2019 IEEE Energy Convers Congr Expo ECCE 2019 2019:569–75. doi: 10.1109/ECCE.2019.8912594.
[6] Greene DL, Ogden JM, Lin Z. Challenges in the designing, planning and deployment of hydrogen refueling infrastructure for fuel cell electric vehicles. ETransportation 2020;6:100086. https://doi.org/10.1016/j.etran.2020.100086.
[7] Ajanovic A, Haas R. Prospects and impediments for hydrogen and fuel cell vehicles in the transport sector. Int J Hydrogen Energy 2021;46:10049–58. https://doi.org/10.1016/j.ijhydene.2020.03.122.
[8] Mahmoud M, Garnett R, Ferguson M, Kanaroglou P. Electric buses: a review of alternative powertrains. Renew Sustain Energy Rev 2016;62:673–84. https://doi.org/10.1016/j.rser.2016.05.019.
[9] Thomas CE. Fuel cell and battery electric vehicles compared. Int J Hydrogen Energy 2009;34:6005–20. https://doi.org/10.1016/j.ijhydene.2009.06.003.
[10] Manoharan Y, Hosseini SE, Butler B, Alzhahrani H, Senior BTF, Ashuri T, et al. Hydrogen fuel cell vehicles; current status and future prospect. Appl Sci 2019;9:2296. https://doi.org/10.3390/app9112296.
[11] Daud WRW, Rosli RE, Majlan EH, Hamid SAA, Mohamed R, Husaini T. PEM fuel cell system control: a review. Renew Energy 2017;113:620–38. https://doi.org/10.1016/j.renene.2017.06.027.
[12] Coppo M, Siegel NP, Spakovsky MR vo. On the influence of temperature on PEM fuel cell operation. J Power Sources 2006;159:560–9. doi: 10.1016/j.jpowsour.2005.09.069.
[13] Mekhilef S, Saidur R, Safari A. Comparative study of different fuel cell technologies. Renew Sustain Energy Rev 2012;16:981–9. https://doi.org/10.1016/j.rser.2011.09.020.
[14] Zhang J, Zhang L, Sun F, Wang Z. An overview on thermal safety issues of lithium-ion batteries for electric vehicle application. IEEE Access 2018;6:23848–63. https://doi.org/10.1109/ACCESS.2018.2824838.
[15] Petzl M, Kasper M, Danzer MA. Lithium plating in a commercial lithium-ion battery - a low-temperature aging study. J Power Sources 2015;275:799–807. https://doi.org/10.1016/j.jpowsour.2014.11.065.
[16] Yang Y, Bilgin B, Kasprzak M, Nalakath S, Sadek H, Preindl M, et al. Thermal management of electric machines. IET Electr Syst Transp 2017;7:104–16. https://doi.org/10.1049/iet-est.2015.0050.
[17] Zhao Z, Wang T, Zhang B, Wang Y, Bao C, Ji Z. Analysis of an integrated thermal management system with a heat-pump in a fuel cell vehicle. AIP Adv 2021:11. https://doi.org/10.1063/5.0056364.
[18] Zhang Y, Zhang C, Huang Z, Xu L, Liu Z, Liu M. Real-time energy management strategy for fuel cell range extender vehicles based on nonlinear control. IEEE Trans Transp Electrif 2019;5:1294–305. https://doi.org/10.1109/TTE.2019.2958038.
[19] Tian Z, Gan W, Zhang X, Gu B, Yang L. Investigation on an integrated thermal management system with battery cooling and motor waste heat recovery for electric vehicle. Appl Therm Eng 2018;136:16–27. https://doi.org/10.1016/j.applthermaleng.2018.02.093.
[20] Farsi A, Rosen MA. PEM fuel cell-assisted lithium ion battery electric vehicle integrated with an air-based thermal management system. Int J Hydrogen Energy 2022;47:35810–24. https://doi.org/10.1016/j.ijhydene.2022.08.153.
[21] Yang Q, Zeng T, Zhang C, Zhou W, Xu L, Zhou J. Modeling and simulation of vehicle integrated thermal management system for a fuel cell hybrid vehicle. Energy Convers Manag 2023;278:116745. https://doi.org/10.1016/j.enconman.2023.116745.
[22] Xu J, Zhang C, Fan R, Bao H, Wang Y, Huang S, et al. Modelling and control of vehicle integrated thermal management system of PEM fuel cell vehicle. Energy 2020;199:117495. https://doi.org/10.1016/j.energy.2020.117495.
[23] Xing L, Xiang W, Zhu R, Tu Z. Modeling and thermal management of proton exchange membrane fuel cell for fuel cell/battery hybrid automotive vehicle. Int J Hydrogen Energy 2022;47:1888–900. https://doi.org/10.1016/j.ijhydene.2021.10.146.
[24] Kim S, Jeong H, Lee H. Cold-start performance investigation of fuel cell electric vehicles with heat pump-assisted thermal management systems. Energy 2021;232:121001. https://doi.org/10.1016/j.energy.2021.121001.
[25] Li L, Gao S, Wang B, Li C, Wang Y, Sun B, et al. Analysis of cooling and heating characteristics of thermal management system for fuel cell bus. Int J Hydrogen Energy 2022. https://doi.org/10.1016/j.ijhydene.2022.07.083.
[26] Tran M-K, DaCosta A, Mevawalla A, Panchal S, Fowler M. Comparative study of equivalent circuit models performance in four common lithium-ion batteries: LFP, NMC, LMO, NCA. MDPI Batter 2021;7. doi: 10.3390/ batteries7030051.
[27] Broatch A, Olmeda P, Bares P, Aceros S. Integral thermal management studies in winter conditions with a global model of a battery-powered electric bus. Energies 2023;16. https://doi.org/10.3390/en16010168.
[28] ASHRAE. 2021 ASHRAE Handbook: fundamentals. SI Edition. 2021.
[29] König A, Mayer S, Nicoletti L, Tumphart S, Lienkamp M. The impact of HVAC on the developoment of autonomous and electric vehicle concepts. Energies 2022;15:441. https://doi.org/10.3390/en15020441.
[30] ASHRAE. 2019 ASHRAE Handbook - HVAC Applications. SI Edition. 2019.
[31] Arrigoni A, Arosio V, Peressut AB, Latorrata S, Dotelli G. Greenhouse gas implications of extending the service life of PEM fuel cells for automotive applications: a life cycle assessment. Clean Technol 2022;4:132–48. https://doi.org/10.3390/cleantechnol4010009.
[32] El-Fergany AA, Hasanien HM, Agwa AM. Semi-empirical PEM fuel cells model using whale optimization algorithm. Energy Convers Manag 2019;201:112197. https://doi.org/10.1016/j.enconman.2019.112197.
[33] Li Q, Chen W, Liu Z, Li M, Ma L. Development of energy management system based on a power sharing strategy for a fuel cell-battery-supercapacitor hybrid tramway. J Power Sources 2015;279:267–80. https://doi.org/10.1016/j.jpowsour.2014.12.042.
[34] Barbir F. PEM fuel cells: theory and practice. Vol. 64. 2nd ed. 2012.
[35] Wei L, Mohmed A, Jiang F. Effects of reactants/coolant non-uniform inflow on the cold start performance of PEMFC stack. Int J Hydrogen Energy 2020;45:13469–82. https://doi.org/10.1016/j.ijhydene.2020.03.031.